CK2 inhibitor CX-4945 targets EWS-FLI1 protein abundance and shows anti-tumor activity in metastatic mouse models of Ewing Sarcoma

Muhammad Daniyal[1], Rajesh Rajaiah[1], Marudhu Pandiyan Shanmugam[1], Sholler Chloe[2], Hengst Jeremey[2], Abhinav Beeravally Nagulapally[2], Giselle Saulnier Sholler[2], Yasin Uzun[1], Hannah Valensi[1], and Chandrika Gowda Behura[1*]

[1]Department of Pediatrics, Pennsylvania State University College of Medicine, Hershey, PA USA

[2]Penn State Health Children's Hospital and Penn State College of Medicine, Hershey, PA USA

***Corresponding Author:** Dr. Chandrika Gowda Behura

Email: cxg40@psu.edu;

Tel.: 717-531-6012;

Fax: 717-531-4789

Competing interest statement: This work is supported by the National Center for Advancing Translational Sciences (KL2 TR002015) (C.G.); Hyundai Hope on Wheels Scholar Grant (C.G.); Four Diamonds Fund of the Pennsylvania State University College of Medicine; JohnWawrynovic Leukemia Research Scholar Endowment (C.G.); St. Baldrick's Foundation; and Rally Foundation.

Institutional Review Board Statement: All the animal experiments were conducted in the Developmental Therapeutics Preclinical Core facility at Penn State University College of Medicine under protocols approved by the Institutional Animal Care and Use Committee at Penn State Hershey, Hershey, PA (IACUC # PROTO201901034). De-identified patient samples were provided by collaborators at Penn State Cancer Institute, at Penn State University College of Medicine (Hershey, PA, USA), and used in compliance with Institutional Review Board regulations.

Informed Consent Statement: Not applicable.

Data Availability Statement: The datasets analyzed and novel reagents used during the current study is available from the corresponding author upon request and after material transfer agreement.

Acknowledgments: The authors would like to thank

Conflicts of Interest: The authors declare no conflict of interest.

Figures: 7 main figures, 5 supplementary figures

Tables: 4 supplementary tables

Abstract:

Ewing sarcoma (ES) is a highly aggressive bone cancer. EWS-FLI oncogenic fusion protein is detected in more than 85% of cases and is indispensable for ES tumor survival and progression. Casein kinase II (CK2) is a serine/threonine kinase that plays an essential role in apoptosis, DNA damage repair, and the cell cycle. CSNK2A1 is highly expressed in ES and associated with metastatic disease and poor 5-year overall survival. CK2 is shown to phosphorylate and stabilize several transcription factors, including EWS-FLI1. We demonstrate that genetic and pharmacological inhibition of CK2 decreases protein abundance of EWS-FLI1 by increased ubiquitination and proteasomal degradation. Clinical-grade inhibitor of CK2, CX-4945 (silmitasertib), shows in vitro cytotoxic activity in a series of ES tumor organoids and patient-derived xenograft cells. We also demonstrate anti-tumor activity of single agent CX-4945 using metastatic xenograft models of Ewing sarcoma. We also show decreased lung metastases in mice treated with CX-4945. CX-4945 showed synergistic cytotoxic activity with Temozolamide and Irinotecan. CX-4945 is currently being tested in a Phase 1 study to evaluate the safety and

tolerability in combination with chemotherapy for the treatment of pediatric colloid tumors, including Ewing sarcoma. The preclinical studies reported here support the clinical studies evaluating the efficacy of CX-4945 for the treatment of Ewing sarcoma.

Introduction

Ewing Sarcoma is the second most common bone tumor in children and an aggressive cancer (1). Nearly 85% of EWS harbor EWS-FLI1 fusion oncogene (2, 3). Metastatic and recurrent Ewing sarcoma have dismal overall survival at 5 years of less than 30% (4, 5). Current standard of care therapy involves local control with surgery, radiation, and multi-agent chemotherapy given in compressed intervals (6). There is an urgent need for novel therapeutic strategies that are both safe and effective and can be quickly translated to the clinic.

EWS-FLI1 drives aggressive phenotype and is the strongest known negative predictive factor in EWS (4, 5). EWS-FLI1 transcription factor regulates widespread target gene expression via chromatin remodeling (7-9). EWS-FLI1 is a tumor-specific translocation that is an excellent molecular target for therapy, but direct targeting of the EWS-FLI1 protein has been challenging for decades, and new strategies are needed (10).

Casein Kinase 2 (CK2) is a constitutively active, ubiquitously present serine/threonine kinase required for normal cellular processes and commonly overexpressed in cancer (11-13). CK2 is a validated anti-cancer target in more than twenty human cancers, including pediatric cancers(14-19). CX-4945 (Silmitasertib) is an orally bioavailable, ATP-competitive, selective small-molecule CK2 inhibitor with favorable pharmacokinetic properties (20-23). CX-4945 has shown safety and tolerability in four completed Phase I trials in adult cancer. We are currently evaluating the safety and tolerability of silmitasertib in combination with chemotherapy in pediatric patients with solid tumors (NCT06541262). Phase 1 study is open for enrollment in over 8 centers across USA. We

are currently at the highest dose level with manageable GI toxicity and anticipate completion of Phase 1 within the next 6-9 months. We also saw a partial response in 2 out of 8 patients.

CK2 as an anti-cancer target:

Casein kinase II (CK2) is a serine/threonine kinase essential for normal cellular processes and overexpressed in many cancers(25-27). CK2 is most often present as a tetramer composed of two catalytic (α and α′) and two regulatory subunits (β). A consensus CK2 phosphorylation sequence is distinct from other kinases and contains acidic amino acids (Ser/Thr-x-x-Glu/Asp) (28). CK2 is multifunctional in cell cycle regulation, signal transduction, transcriptional control, angiogenesis, apoptosis, and inflammation, and cellular processes (11, 25, 29). CK2 is responsible for the phosphorylation of >20% of the human kinome, more than any other kinase enzyme (30, 31). Studies have shown that cancer cells depend more on high CK2 than their normal tissue counterparts for survival and proliferation (32). Therefore, targeted inhibition of CK2 is an effective and safe therapeutic strategy in cancer (33).

The commonly identified phosphorylation substrates of CK2 implicated in cancer include AKT, STAT3, PTEN, IKAROS, MYC, and TP53(17). CK2 is ubiquitously distributed in multiple cell types' cytoplasmic and nuclear compartments. CK2 is constitutively active and does not need phosphorylation by other kinases for activation. There are no recurrent activating genetic alterations in the CSNK2A1 gene encoding the CK2 enzyme. This is unlike several other oncogenic proteins, such as PI3K, PTEN, RAF, and RAS, where alterations in encoding genes lead to an altered molecule concomitant with a dysregulation of their pathways. While no mutations in CSNK2A1 have been reported, CK2 expression and enzyme activity are elevated in over 25 cancers of diverse genetic backgrounds, including breast, lung, prostate, colorectal, sarcomas, EWS, and leukemia (34, 35). High CK2 activity is attributable to overexpression of the

molecule. Moreover, the elevation of CK2 in cancer tissues has frequently been linked to disease progression, drug resistance, and poor prognosis. Given the widespread overexpression of CK2 in multiple cancers and its role in numerous non-oncogenic processes required to sustain the cancer phenotype, a selective inhibitor of CK2 is an attractive targeted approach to treating cancer.

Study drug - Silmitasertib

Silmitasertib (CX-4945) is a tetracyclic synthetically derived small molecule carboxylate acid salt that exhibits potent and highly selective inhibition of CK2 (23, 36). The biological activity of CX-4945 has been evaluated in both in vitro and in vivo studies(37). Key attributes of CX-4945 include potent inhibition of CK2 enzymatic activity and a highly selective kinase profile (21). Evaluation of CX-4945 in cell viability assays revealed broad-spectrum anti-proliferative activity in cancer cell lines and direct suppression of DNA repair pathways(38, 39). CX-4945 is a potent inhibitor with K(i) values in the low nanomolar range and high selectivity (49 of 250 kinases) versus other kinases (37).

Here, we report preclinical evidence of anti-tumor activity of CX-4945 in Ewing sarcoma xenograft models and describe its mechanism of action.

Materials and Methods:

Cell culture and treatment

The human Ewing's Sarcoma (EWS) cell lines A673 and SK-ES-1 were obtained from ATCC and cultured in Minimum Essential Medium α (MEM α) (Gibco) supplemented with 10% FBS and 10% penn/strap. PDX cell lines were cultured in same media as cell liens. Cell lines were routinely authenticated by STR profiling (Promega, Madison, Wisconsin, USA) and monitored for mycoplasma contamination. Each frozen aliquot was used and propagated for no more than 30 passages.

Patient samples

All primary EWS samples obtained from BCC and cultured in MEM alpha supplemented with 10% FBS and 10% penn/strap.

Drugs and Reagents

The CK2 inhibitor CX-4945 sodium salt was provided by Senhwa Biosciences. CX-4945, Temozolomide and Irinotecan were purchased from MedChem Express (Monmouth Junction, NJ, USA).

Wound repair

Cells were seeded into 6-well plate and waited for the 90 to 100% confluency. After that using sterile pipette tip, wound was created across the monolayer of cells. Uniform wound was created in all the conditions. All the wells were washed with PBS to remove the detached cells. Media was replaced with containing DMSO for Vehicle and CX-4945 with difference concentration for treatment groups. Closure of wound was measured over the time e.g., 0, 6, 12, 24, 48, 72 hours using microscope. Captures images were analyses for wound closure distance as % using the Image J software.

Migration assay

EWS cells were serum starved for 18 h. Subsequently, $5X10^4$ cells in 500 ml of serum-free MEM alpha media were added to the upper chamber of each insert (Transwell® Permeable 6.5mm insert, 8.0µM pore size, TC treated) in a 24 well plate. 600 µl of complete media (MEM alpha with 10% FBS) were added to the lower chambers. Cell invasion chambers were incubated at 37°C, 5% CO_2 for up to 48 h. Then, the media in the upper chamber was aspirated and any remaining media was gently removed with a cotton bud, taking care not to damage the bottom membrane of the Transwell insert. Migrated cells were fixed with 0.5% paraformaldehyde in PBS for 30 mins and

subsequently stained with 0.1% crystal violet dye for 10 mins, followed by washing with water for 3 to 5 times prior to air dying. Cells were viewed under light microscope, then 5 to 8 microscopic field were imaged and counted using Image J software.

Invasion assay

Invasion assays were performed in a similar manner as the migration assays. However, Transwell inserts were coated with Corning® Matrigel® Basement Membrane Matrix (Catalog #356234, Lot #3131001) prior to adding EWS cells. The Matrigel was diluted with serum media in 1:1 ratio. 80µL of diluted Matrigel matrix coating solution was added to each Transwell® insert (Corning Product #3422) and incubated at 37° C for two hours to facilitate polymerization. EWS cells were incubated for 48 hours prior to staining. The remaining step of the protocol was identical to that of the migration assays.

Incucyte cell proliferation and Apoptosis assays

EWS cells were seeded at 5000 cells/well in 96 well plates for proliferation assay. Live-cell phase contrast images were obtained using a 10× objective lens (five images per well), and cell confluence was analyzed using IncuCyte Live Cell Analysis (v2019B) software. For apoptosis assay, EWS cell lines or PDX of 10,000 cells/well (50ul/well) were seeded in 96-well plates, and after 12–14 hours, Caspase 3/7 Dye for Apoptosis Green (Sartorius, Cat # 4440; 50ul/well with media and drug) was added. Images were obtained every 2 hours for 120 hours, and relative apoptosis was quantified using the Basic Analyzer module in Incucyte Analysis software (Sartorius 9600-0012). For apoptosis analysis in Scramble and Sh-CSNK2A1 cells, Caspase 3/7 Dye for Apoptosis Red (Sartorius, Cat # 4704) was used.

RT-qPCR

Total RNA was isolated using TRIzol (Thermo Fisher Scientific, Waltham, MA, USA) and reverse -transcribed into cDNA using iScript cDNA Synthesis Kit (Bio-Rad Laboratories Inc., Richmond, CA). cDNA amplification was performed with PowerTrack SYBR Green Master Mix (Applied Biosystems, Vilnius, Lithuania). GAPDH was used as an internal control gene for normalization. The thermal cycling program consisted of the following steps: denaturation at 94 °C for 30 s and annealing/extension for 30 s at 60 °C for a total of 40 cycles. For the sequences of the used primers, see table S2.

Immunoblotting

Cells were lysed in RIPA-buffer (50 mM Tris-HCl pH 7.4, 150 mM NaCl, 1% Nonidet P-40, 0.5% Na-Deoxycholate, 0.1 % Sodium Dodecyl Sulfate), supplemented with protease inhibitor and phosphatase inhibitor. The protein concentration was normalized after performing a bicinchonic acid assay (BCA, Thermo Scientific). 10-20 µg per lysate were separated on Bolt™ 4-20% Bis-Tris Plus gels (Bio-red) and subsequently blotted to a polyvinylidene fluoride (PVDF)-membrane (Bio-red). The primary antibodies are listed in table S. Primary antibodies were detected with anti-mouse-HRP or anti-rabbit-HRP (both cell signaling), followed by detection using Pierce™ ECL Western Blotting Substrate (Thermo Scientific). The quantification of the protein bands was assessed using ImageJ software.

RNA Sequencing Analysis:

Paired-end RNA sequencing reads were trimmed using Trimmomatic with the TruSeq3_PE.fa adapter sequences to remove adapters and low-quality bases. The trimmed reads were then aligned to the corresponding reference genome (hg38 for human samples and mm39 for mouse samples) using the STAR aligner. Gene-level quantification was performed based on the Gencode annotation, using version 38 for human samples and version 36 for mouse samples. Gene

expression levels were normalized and expressed as fragments per kilobase of transcript per million mapped reads (FPKM) using Cufflinks. For downstream analyses, genes with an FPKM value greater than 1.0 in at least two samples within either experimental group were retained.

Raw read counts were obtained using the feature Counts function from the Rsubread package. Differential expression analysis was conducted using edgeR, where a quasi-likelihood negative binomial generalized log-linear model was fitted to the data via the glmQLFTest function. Prior to modeling, raw count data were normalized using the trimmed mean of M-values (TMM) method. The Benjamini–Hochberg (BH) procedure was applied for multiple testing correction, and genes with an adjusted p-value below 0.05 were considered significantly differentially expressed.

Gene set enrichment analysis (GSEA) was performed using GSEA software, with normalized FPKM values as input. Functional enrichment analysis via Metascape was conducted using the top 100 upregulated and top 100 downregulated genes, ranked by statistical significance. Visualization of differential expression and pathway enrichment results was performed using the ggplot2, pheatmap, enrichplot, and dplyr packages in R.

Flow cytometry

A673, SK-ES-1, PDX 1460, PDX 755 and PDX 287 were incubated with Zombie Aqua Fixable Viability dye (Biolegend, Cat #423102) to distinguish Live/Dead cells before primary antibody staining. Cells were incubated with Blocking Solution. Cells were then incubated with respective primary antibodies cocktail (CD99, CD133 and SEEA4) for 30 minutes on ice. After washing twice, cells were suspended in FACS buffer and analyzed on a FACS Calibur flow cytometer (Becton Dickinson, Heidelberg, Germany). Flow antibodies details are mentioned in tableS4.

Animal studies

A673 and PDX EWS cell were injected into athymic nude mice on right flank region at a dose of 2500K and 4000k cells per mouse respectively. Total 20 mice randomized into 2 groups, 10 mice per group for each study. Group 1 treated with PBS only, Group 2 treated with CX-4945 100 mg/kg via oral gavage twice daily, treatment continues for the 28 days. Tumor volume and body weight measured twice weekly. After the 28 days or when tumor reached the end point mice were sacrifices and tumor and lung tissues were collected for H&E and IHC staining and single cell from both tissues collected for western blot. CBC and chemistry were performed from peripheral blood collected at the time of sacrifices.

Pathological tissue staining and H&E analysis

Mouse tumor tissues were obtained, embedded in paraffin, and sectioned at a thickness of 4 μm after being fixed in formalin. Afar deparaffinization, rehydration and antigen retrieval, the sections were incubated with a 3% H2O2 solution for 10 min at room temperature in the dark. Afar the sections were washed three times with PBS, they were incubated with 5% goat serum at room temperature for 1 h. Ten, the tumor tissue sections were incubated with antibodies against specific markers including Ki67 (1:200), CD99 (1:100), at 4 °C overnight. The sections were washed and subsequently incubated with a horseradish peroxidase-labelled secondary antibody solution at room temperature for 30 min and visualized using a DAB color development kit. After three minutes of staining the nuclei with hematoxylin, images of the histological specimens were captured using a microscope Versa ver 8. H&E analysis was done. Mitotic figures were counted as a total number identified over 10 consecutive high-power (400x) microscope fields. Counting started at the area with the most mitotic figures. Variance in the mitotic figures may be a result of tumor cell health, blood supply, mutations, effect of treatment, etc. The number may also be artifactually lowered in areas with very high necrosis. Degree of necrosis was quantified as a

percentage of the tissue as well as given an overall severity score to assist interpretation. The amount of fibrovascular stroma was also evaluated; the degree of fibrovascular tissue may indicate the ability of the tumor to induce vascularization.

Statistics

Statistical analyses were performed using GraphPad Prism 9 (GraphPad Software, La Jolla, CA). For Kaplan-Meier analysis, log-rank tests were used. For comparisons between 2 groups, 2-tailed Student t-tests were performed, for comparisons between more than 2 groups, two-way analysis of variance (ANOVA) with Tukey, Šidák or Dunnett's multiple comparison post-hoc tests were used as indicated in each figure legend. A value of $P<0.05$ was considered statistically significant. The significance level of P values is indicated by asterisks (*$P<0.05$; **$P<0.01$; ***$P<0.001$; ****$P<0.0001$; ns, not significant).

Results:

CK2 in Ewing Sarcoma: High expression of CSNK2A1 and CK2 activity is noted in Ewing sarcoma. Metastatic EWS has high CSNK2A1 expression compared to localized EWS. CSNK2A1 high-expressing EWS has significantly poor overall and event-free survival.

Studies report that EWS protein is phosphorylated by CK2 (at Ser325)(10, 40). EWS-FLI fusion oncoprotein is detected in more than 85% of Ewing sarcoma and is indispensable for Ewing tumor survival and growth. Forced expression of CK2 in 293T cells increased EWS-FL1 protein (40). CX-4945 induce apoptosis in Ewing sarcoma PDX patient derived xenograft (PDX) cell lines (n = 20). We used two EWS-FLI1 fusion driven EWS cell lines A763 and a PDX cell line obtained from BCC biorepository. CX-4945 treatment significantly decreases the migration and invasion potential of treated cells. CX-4945 treatment decreases CK2 substrate phosphorylation (a measure

of CK2 activity), EWS-FLI protein level, GLI1 (EWS-FLI target), BCL-XL (anti-apoptotic protein), phosphor Akt (serine 129), a specific substrate of CK2. To analyze, differentially expressed genes (DEG) and signaling pathways altered by CK2α depletion, specifically, EWS-FLI1 target genes, we performed whole transcriptomic sequencing (RNA-seq) of CX-4945 treated and shCK2 treated A673 and PDX cells and noted that there is significant downregulation of EWS-FLI1 signature genes including GLI1, EZH2. Further, qPCR analysis showed dose dependent decrease in GLI1 following CX-4945 treatment. We then tested ubiquitination-specific K48 marker following CX-4945 treatment, which showed a significant increase in ubiquitination of protein, suggesting ubiquitination followed by proteasomal degradation of EWS-FLI1 is induced by CX-4945 exposure. In order to determine the effect of molecular inhibition of CK2 on phenotype and gene expression, we depleted CK2α in the A673 cell line using short hairpin RNA (shRNA) directed towards the CK2α (CSNK2A). After confirming CK2α mRNA and protein depletion (qPCR and western blot), we characterized the phenotype in vitro and in vivo. In vitro, CK2-depleted EWS cells proliferated slowly, were more sensitive to irinotecan-induced apoptosis, and showed less transwell migration and invasion potential. EWS cells treated with shCk2α or scramble shRNA were transplanted via subcutaneous and orthotopic into the flank of athymic mice (6 mice per group) to assess in vivo engraftment potential. Small tumor size is noted in CK2-depleted mice. The tumor and lung sections were stained with H&E and evaluated by a pathologist. The mice bearing shCK2-treated EWS tumors also had significantly less lung metastasis.

EWS- FLI1 subcutaneous xenograft models using cell line A673 and patient cells (SL01460 from BCC) were treated with CX-4945 as a single agent for up to 4 weeks. Treatment with CX-4945 alone slowed tumor progression and prolonged survival of treated mice significantly. We measured the CK2 substrate and EWS-FLI1 in the tumors of treated mice and confirmed target inhibition.

Histological evaluation of the tumors from treated and untreated groups by pathologist showed decreased lung micro metastasis islands in treated mice which was also confirmed by CD99 immunohistochemistry. CD99 is an EWS-specific marker.

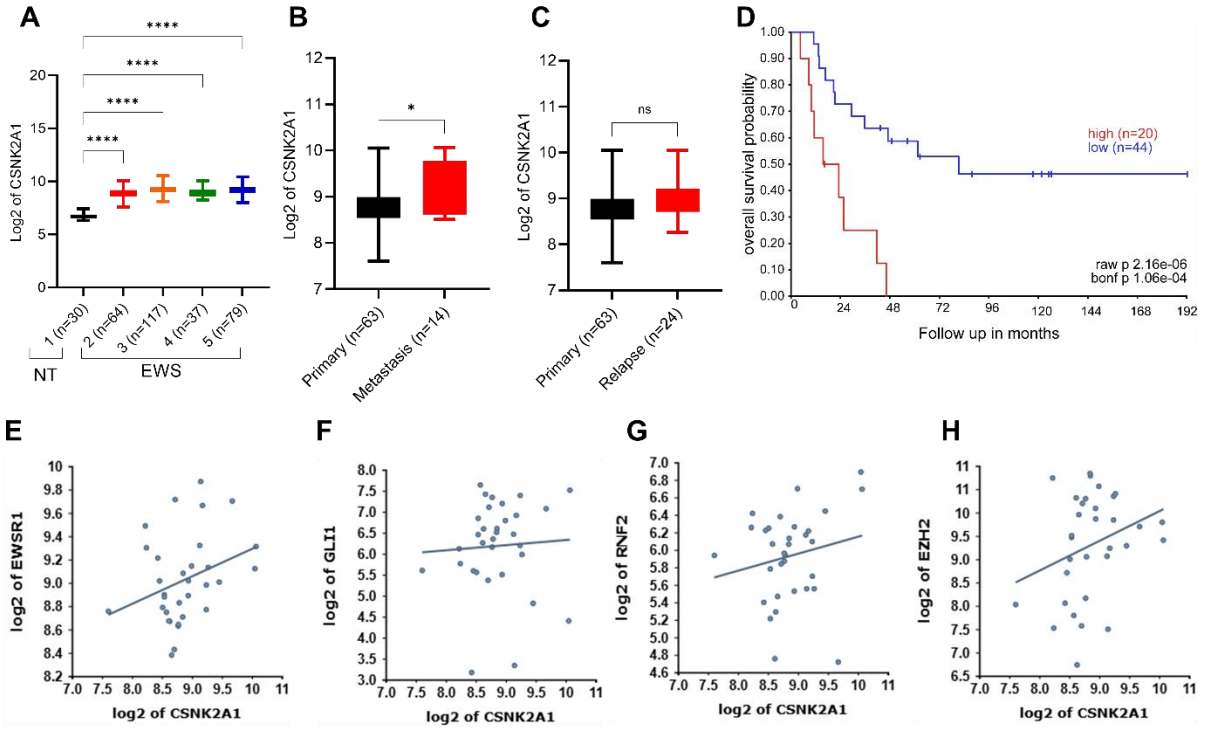
A
Log2 of CSNK2A1
****
****
****
****
1 (n=30)
2 (n=64)
3 (n=117)
4 (n=37)
5 (n=79)
NT
EWS
B
Log2 of CSNK2A1
*
Primary (n=63)
Metastasis (n=14)
C
Log2 of CSNK2A1
ns
Primary (n=63)
Relapse (n=24)
D
overall survival probability
high (n=20)
low (n=44)
raw p 2.16e-06
bonf p 1.06e-04
Follow up in months
E
log2 of EWSR1
log2 of CSNK2A1
F
log2 of GLI1
log2 of CSNK2A1
G
log2 of RNF2
log2 of CSNK2A1
H
log2 of EZH2
log2 of CSNK2A1

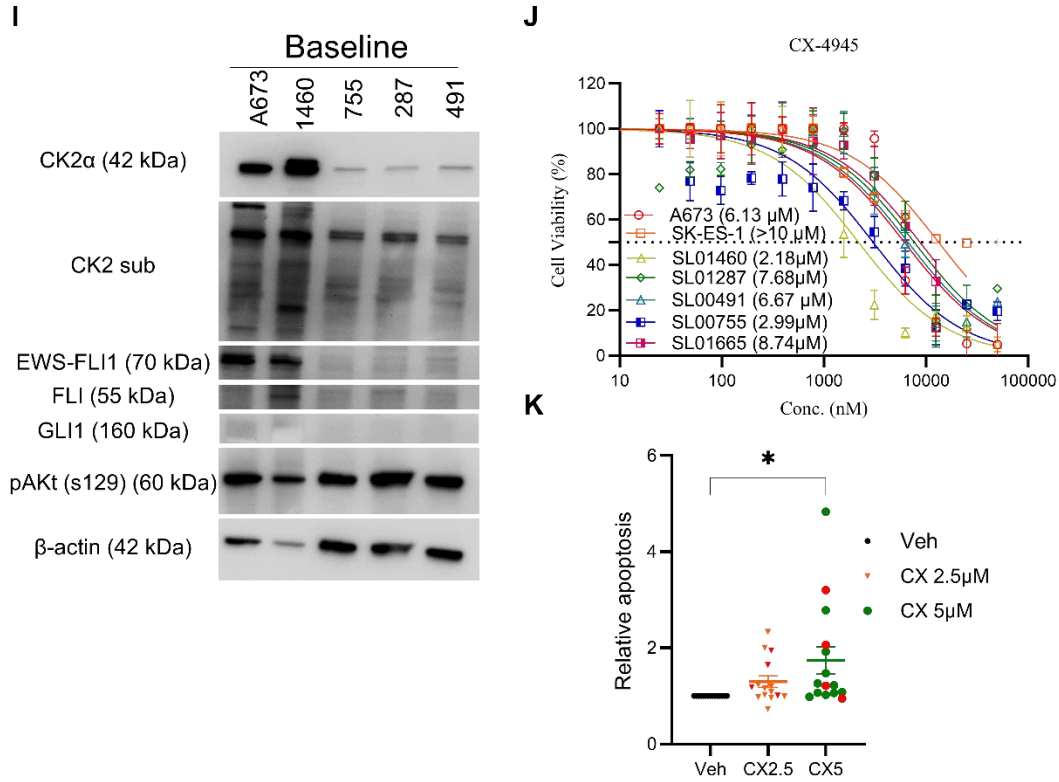
I
Baseline
A673
1460
755
287
491
CK2α (42 kDa)
CK2 sub
EWS-FLI1 (70 kDa)
FLI (55 kDa)
GLI1 (160 kDa)
pAKt (s129) (60 kDa)
β-actin (42 kDa)
J
CX-4945
Cell Viability (%)
A673 (6.13 μM)
SK-ES-1 (>10 μM)
SL01460 (2.18μM)
SL01287 (7.68μM)
SL00491 (6.67 μM)
SL00755 (2.99μM)
SL01665 (8.74μM)
Conc. (nM)
K
Relative apoptosis
*
Veh
CX 2.5μM
CX 5μM
Veh
CX2.5
CX5

Figure 1: CSNK2A1 mRNA expression, baseline protein expression and CX-4945 cytotoxicity on Ewing sarcoma cell line and PDXs (A) comparison of Ewing sarcoma (EWS) patient samples (4 data sets) to normal tissues (NT); **(B)** comparison between primary vs metastasis; and **(C)** primary vs relapse EWS; **(D)** Kaplan-Meyer survival curve for EWS patients with high or low CSNK2A1 expression. **(E-H)** Correlation of CSNK2A1 gene to EWS-FLI1 targeted genes; **(E)** EWSR1, **(F)** GLI1, **(G)** RNF2, and **(H)** EZH2; **(I)** Baseline expression of CK2a and its activity (substrate phosphorylation) and other apoptotic and anti-apoptotic proteins in EWS cell lines and PDXs cells analyzed by Western blotting; **(J)** Cytotoxicity of CX-4945 with different concentration on different EWS cell lines and PDXs cells analyzed by WST reagent after incubating 48hrs; **(K)** Relative apoptosis of EWS PDXs (n=15) were analyzed by incucyte, green optimal count for different PDX cells was recorded at 48 h and relative apoptosis was calculated using vehicle-treated cell apoptosis as 1.

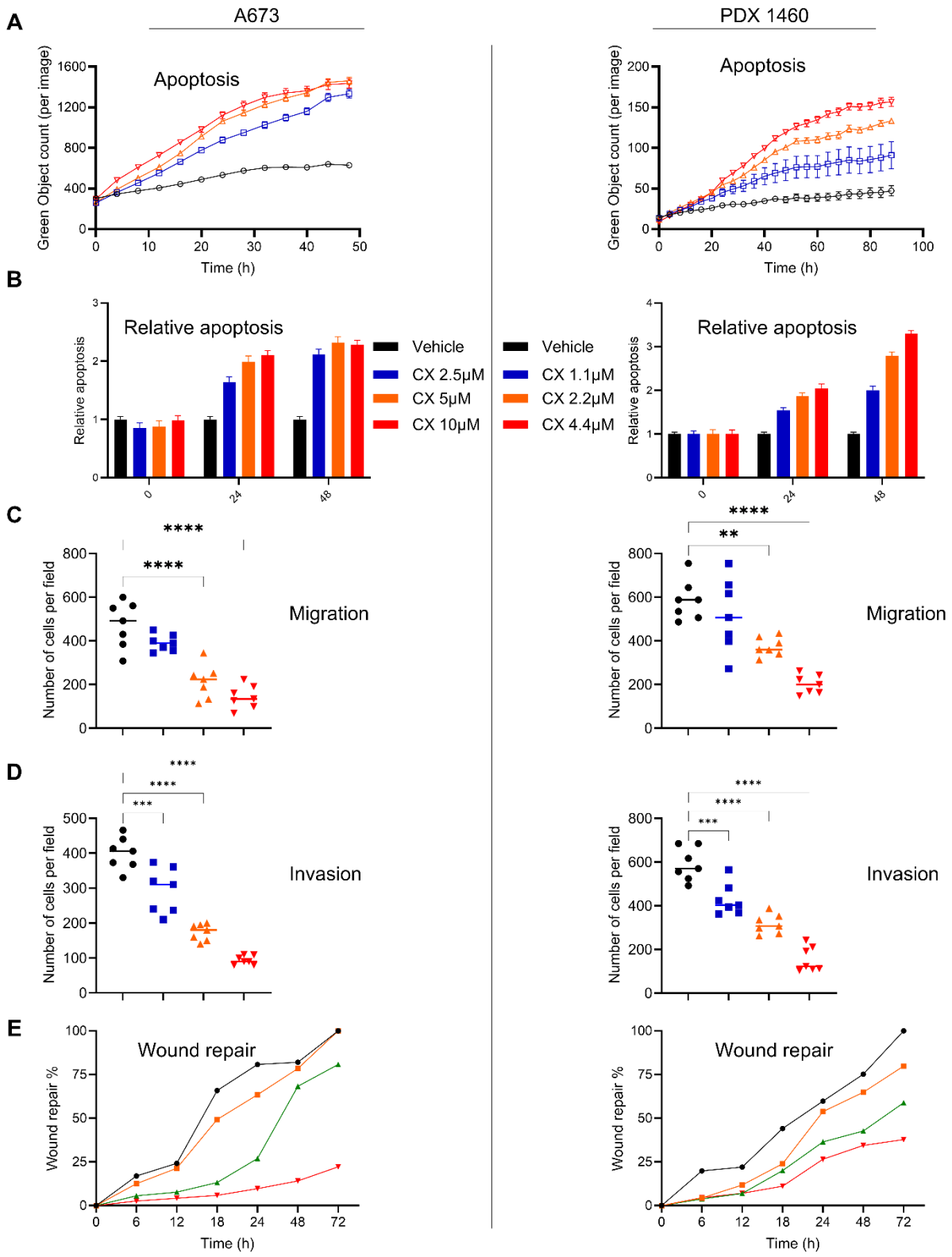
A
A673
PDX 1460
Apoptosis
Green Object count (per image)
Time (h)
B
Relative apoptosis
Vehicle
CX 2.5μM
CX 5μM
CX 10μM
CX 1.1μM
CX 2.2μM
CX 4.4μM
C
Migration
Number of cells per field
D
Invasion
E
Wound repair
Wound repair %

Figure 2: The effects of CX-4945 on EWS cell line (A673 Left panel) and (PDX 1460 right panel); (A) Green object count/Apoptosis was assessed using Incucyte platform. Graph were made as Increased green optimal count directly proportional to increased apoptosis**. (B)** Green optimal count at different time points was recorded and relative apoptosis was calculated**. (C)** To assess the effect of CX-4945 on migration **(C)** and invasion **(D),** cells were treated in the presence or absence of CX-4945 for 48 h. Migration and invasion were quantitated as number of cells per field from 6-7 different fields under the microscope**. (E)** For scratch healing assay, cells were treated with different concentration of CX-4945 after uniform scratch was made. Wound area/repair was recorded at different time points under the microscope.

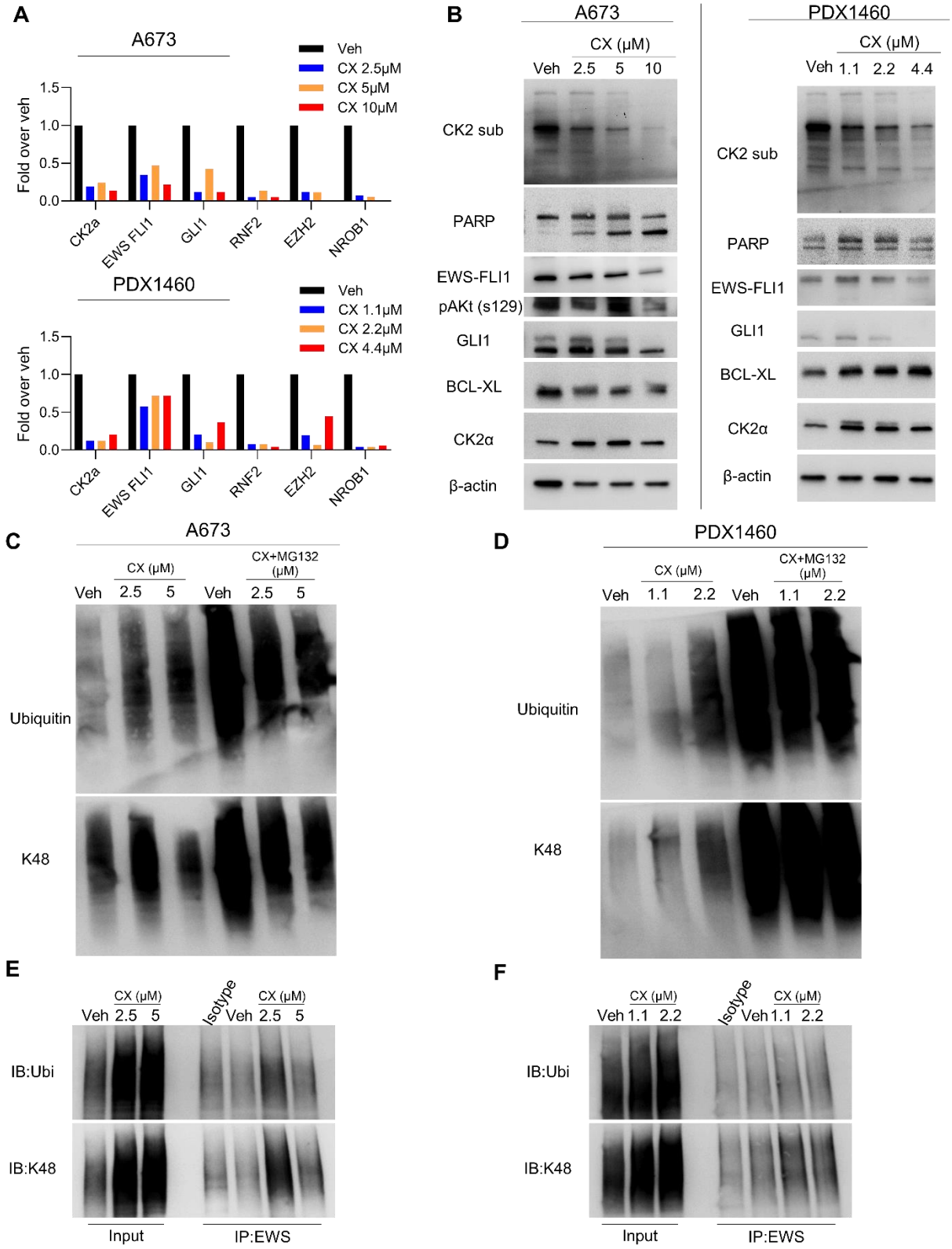
A
A673
Veh
CX 2.5μM
CX 5μM
CX 10μM
Fold over veh
1.5
1.0
0.5
0.0
CK2a
EWS FLI1
GLI1
RNF2
EZH2
NROB1
PDX1460
Veh
CX 1.1μM
CX 2.2μM
CX 4.4μM
B
A673
CX (μM)
Veh 2.5 5 10
CK2 sub
PARP
EWS-FLI1
pAKt (s129)
GLI1
BCL-XL
CK2α
β-actin
PDX1460
CX (μM)
Veh 1.1 2.2 4.4
C
A673
CX (μM)
CX+MG132 (μM)
Veh 2.5 5 Veh 2.5 5
Ubiquitin
K48
D
PDX1460
CX (μM)
CX+MG132 (μM)
Veh 1.1 2.2 Veh 1.1 2.2
E
CX (μM)
Veh 2.5 5
Isotype
Veh 2.5 5
IB:Ubi
IB:K48
Input
IP:EWS
F
CX (μM)
Veh 1.1 2.2
Isotype
Veh 1.1 2.2

Figure 3: CX-4945 downregulate the EWS-FLI1 targeted mRNA and proteins (A) qRT-PCR data showing the expression of different mRNA related to EWS-FLI1 targets, A673 cells **(upper panel)** and PDX 1460 cells **(lower panel**) were treated with different concentration of CX-4945 and mRNA expression of EWS-FLI1 and its downstream mediators was analyzed after 24hrs by qRT-PCR. **(B)** Western blot data showing the protein expression of different EWS-FLI1 targeted protein, A673 cells **(right panel)** and PDX 1460 cells **(left panel**), cells were treated with increased concentration of CX-4945 for 24 h and whole cell lysates were tested for expression of CK2a and its activity (substrate phosphorylation), EWS-FLI1 and its downstream mediators. **(C-D)** Western blot showing the increase ubiquitination with increasing dose of CX-4945 and blockage of proteasomal degradation with addition of MG132, A673 cells **(C)** and PDX 1460 cells **(D**), cells were treated with increased concentration of CX-4945 in the presence or absence of MG132 for 6 h and whole cell lysates were tested for ubiquitination and K48. **(E-F)** CX-4945 treated and untreated A673 **(E)** and PDX1460 **(F)** whole cell lysate was subjected for co-immunoprecipitation with anti-EWS-FLI1 antibody and blots were probed against total ubiquitin and K48 ubiquitin antibodies.

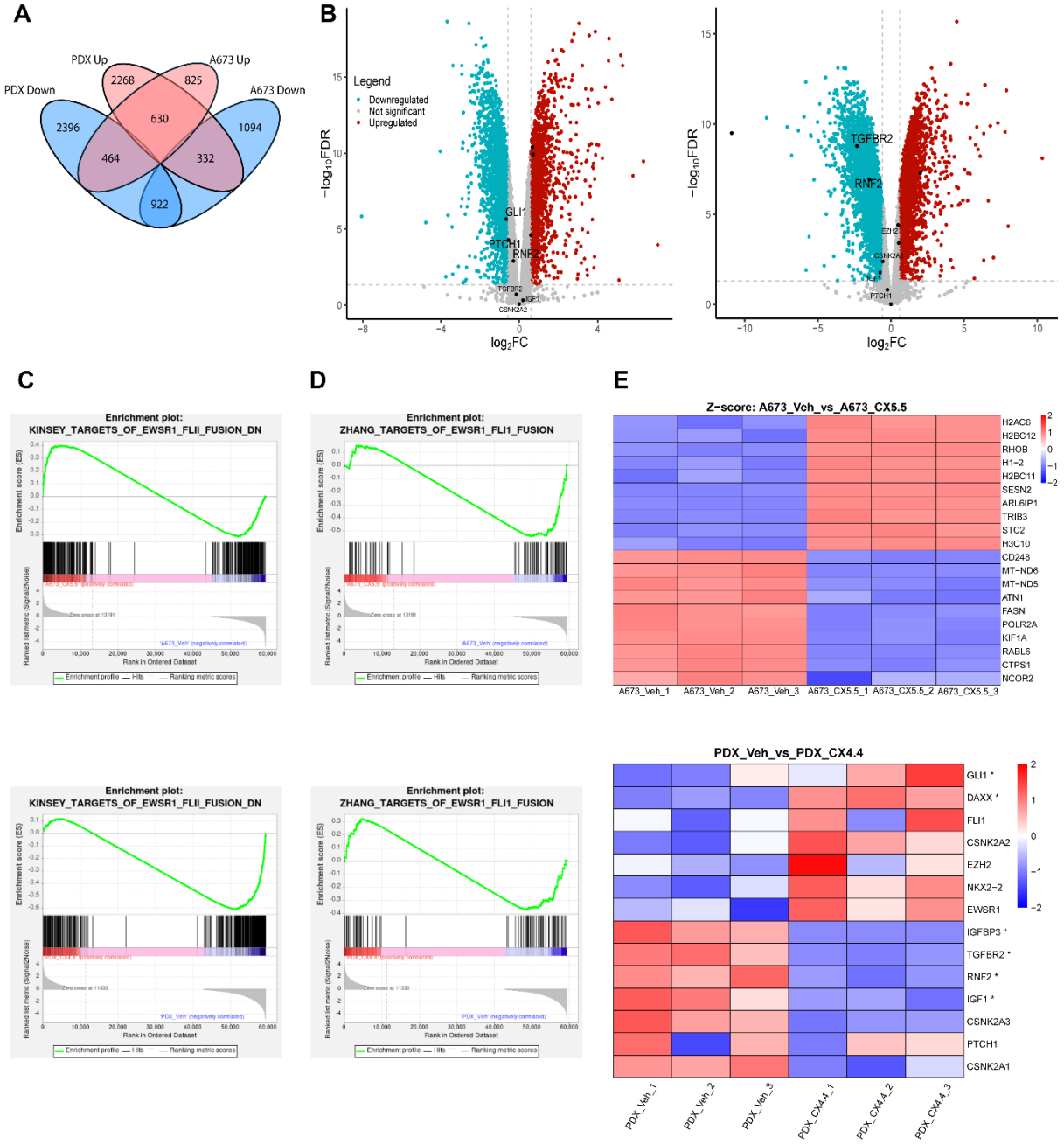
A
PDX Up
A673 Up
PDX Down
A673 Down
2268
825
630
2396
1094
464
332
922
B
Legend
Downregulated
Not significant
Upregulated
−log10FDR
log2FC
GLI1
PTCH1
RNF2
TGFBR2
IGF1
CSNK2A2
EZH2
CSNK2A3
C
Enrichment plot:
KINSEY_TARGETS_OF_EWSR1_FLII_FUSION_DN
Enrichment score (ES)
Rank in Ordered Dataset
Enrichment profile
Hits
Ranking metric scores
D
Enrichment plot:
ZHANG_TARGETS_OF_EWSR1_FLI1_FUSION
E
Z−score: A673_Veh_vs_A673_CX5.5
H2AC6
H2BC12
RHOB
H1−2
H2BC11
SESN2
ARL6IP1
TRIB3
STC2
H3C10
CD248
MT−ND6
MT−ND5
ATN1
FASN
POLR2A
KIF1A
RABL6
CTPS1
NCOR2
A673_Veh_1
A673_Veh_2
A673_Veh_3
A673_CX5.5_1
A673_CX5.5_2
A673_CX5.5_3
PDX_Veh_vs_PDX_CX4.4
GLI1 *
DAXX *
FLI1
CSNK2A2
EZH2
NKX2−2
EWSR1
IGFBP3 *
TGFBR2 *
RNF2 *
IGF1 *
CSNK2A3
PTCH1
CSNK2A1
PDX_Veh_1
PDX_Veh_2
PDX_Veh_3
PDX_CX4.4_1
PDX_CX4.4_2
PDX_CX4.4_3

Figure 4: CX-4945 treatment affects multiple genes involved in EWSR1-FLI1 fusion downstream pathways; (A) Venn diagram showing differentially regulated genes (up and down) in A673 and PDX-1460 cell treated with CX-4945; **(B)** Volcano plots showing significantly upregulated and downregulated genes after CX-4945 treatment A673 cells **(right panel)** and PDX 1460 cells **(left panel)**; **(C)** Gene set enrichment analysis plots of Kinsey targets of EWSRI_FLI1_Fusion after CX-4945 treatment A673 cells **(upper panel)** and PDX 1460 cells **(lower panel)**; **(D)** Gene set enrichment analysis plots of Zhang targets of EWSRI_FLI1_Fusion after CX-4945 treatment A673 cells **(upper panel)** and PDX 1460 cells **(lower panel); (E)** Heat map showing significantly upregulated and downregulated ($p<0.05$; fold change +2.0 and less than or equal to −2.0) genes A673 cells **(upper panel)** and PDX 1460 cells **(lower panel).**

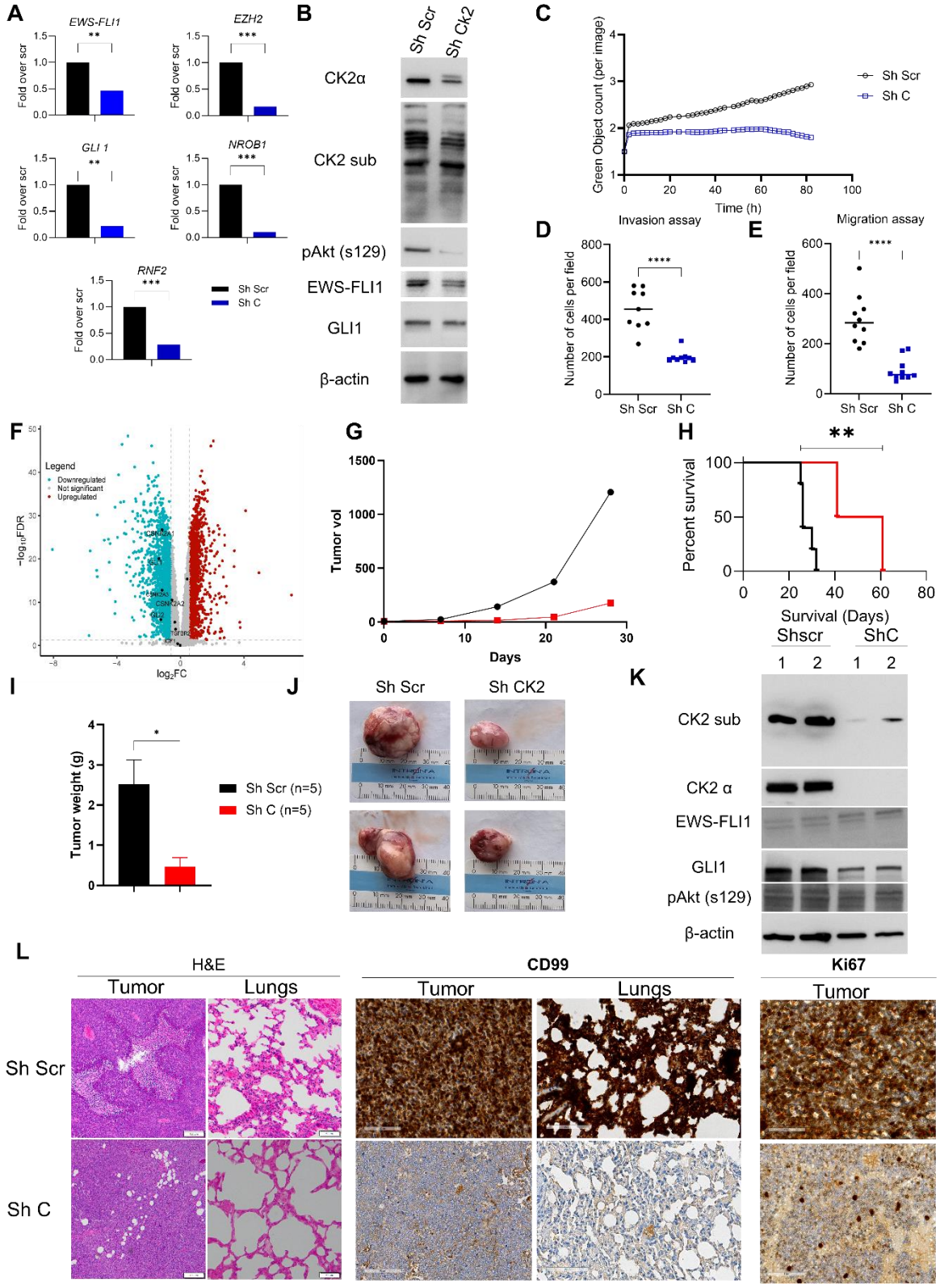
A
EWS-FLI1
EZH2
GLI 1
NROB1
RNF2
Fold over scr
Sh Scr
Sh C
B
Sh Scr
Sh Ck2
CK2α
CK2 sub
pAkt (s129)
EWS-FLI1
GLI1
β-actin
C
Green Object count (per image)
Time (h)
Sh Scr
Sh C
D
Invasion assay
Number of cells per field
Sh Scr
Sh C
E
Migration assay
Number of cells per field
Sh Scr
Sh C
F
Legend
Downregulated
Not significant
Upregulated
−log10FDR
log2FC
G
Tumor vol
Days
H
Percent survival
Survival (Days)
Shscr
ShC
I
Tumor weight (g)
Sh Scr (n=5)
Sh C (n=5)
J
Sh Scr
Sh CK2
K
CK2 sub
CK2 α
EWS-FLI1
GLI1
pAkt (s129)
β-actin
L
H&E
Tumor
Lungs
CD99
Tumor
Lungs
Ki67
Tumor
Sh Scr
Sh C

Figure 5: The consequence of CSNK2A1 genetic inhibition on Ewing sarcoma cell line A673 proliferation, migration/invasion and tumor engraftment in mice; (A-B) Expression of CK2a dependent genes/proteins after transduction of GFP-tagged lentiviral vector expressing scramble (Sh-Scr) and CK2-a specific sh-RNAs (Sh-C) **(A)** gene expression; **(B)** protein expression**; (C)** Comparison of growth proliferation curve between CSNK2A1 knockdown A673 cells compared to cells transduced with scramble shRNA; **(D-E)** Comparison of migration **(D)** and invasion **(E)** between Sh-C A673 cells compared to Sh-Scr shRNA; **(F)** Volcano plots showing significantly upregulated and downregulated genes in CSNK2A1 knockdown A673 cells compared to cells transduced with scramble shRNA; **(G)** Comparison of In vivo tumor volume after injecting the Sh-Scr and Sh-C in nude mice; **(H)** Comparison of survival after injecting the Sh-Scr and Sh-C; **(I-J)** Comparison of tumor weight (I) and tumor pictures **(J)** between Sh-Scr and Sh-C; **(K)** Western blot showing the expression of CK2 substrate and EWS-FLI1 regulated proteins in ***in vivo*** tumor cells; **(L)** H&E and IHC staining showing the difference between Sh-Scr and Sh-C tumor and lungs tissues stained with **H&E left panel**, **CD99 middle panel** and **Ki67 right panel**.

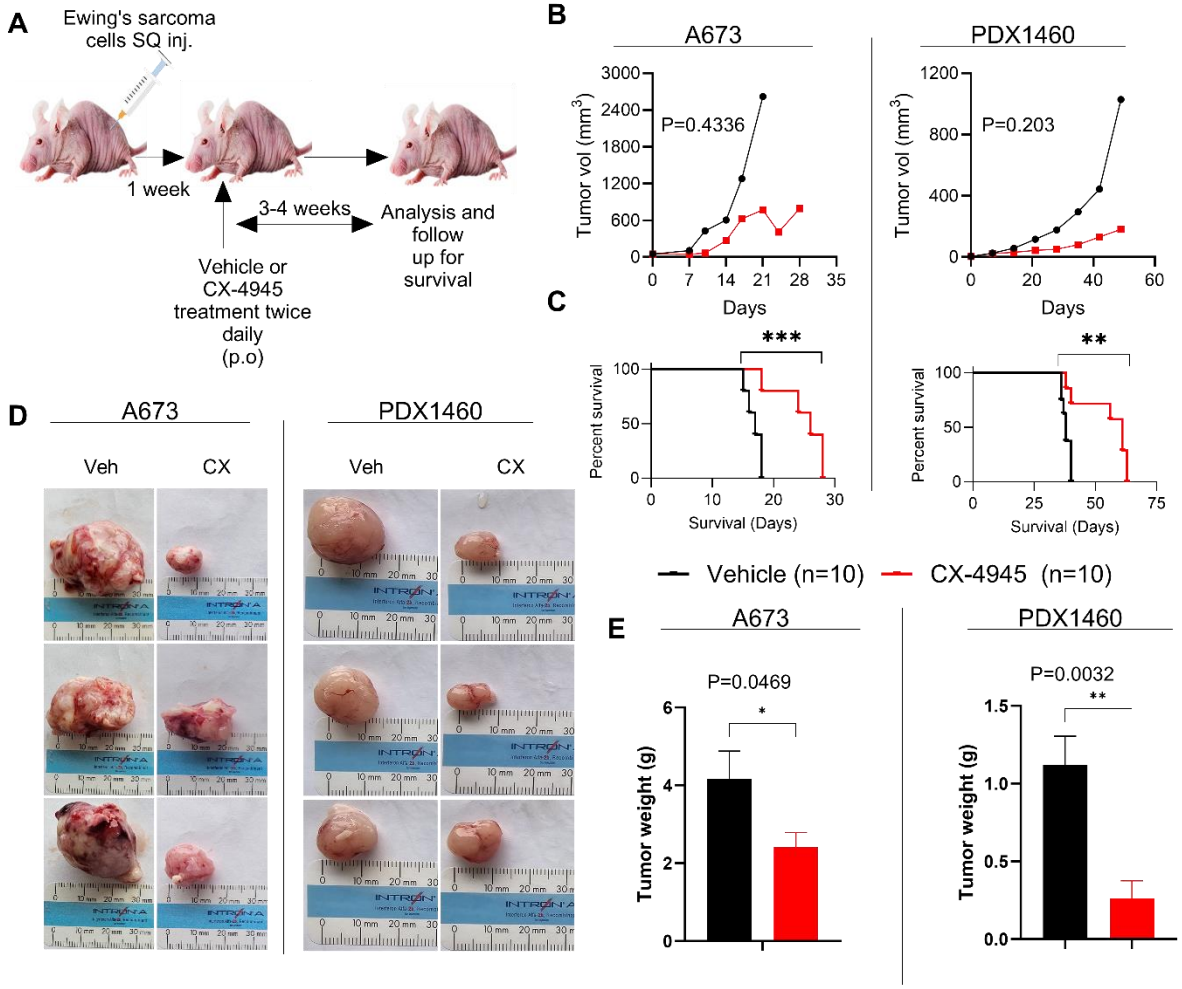
A
Ewing's sarcoma cells SQ inj.
1 week
3-4 weeks
Analysis and follow up for survival
Vehicle or CX-4945 treatment twice daily (p.o)
B
A673
PDX1460
Tumor vol (mm3)
P=0.4336
P=0.203
Days
C
Percent survival
Survival (Days)
***
**
Vehicle (n=10)
CX-4945 (n=10)
D
A673
PDX1460
Veh
CX
E
A673
PDX1460
P=0.0469
P=0.0032
Tumor weight (g)

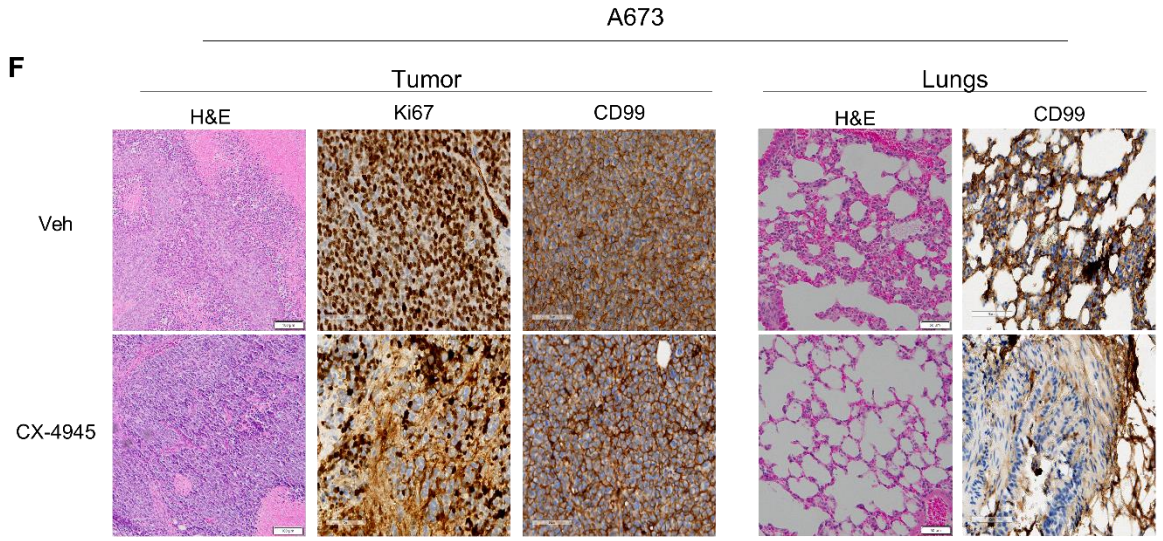
F
A673
Tumor
Lungs
H&E
Ki67
CD99
Veh
CX-4945

Figure 6: Anti-tumor effect of CX-4945 on Ewing sarcoma cell line A673 and PDX 1460 mediated engraftment in athymic mice (A) Schematic diagram showing the development of in vivo mice model using A673 cell line and PDX 1460 EWS; **(B)** Comparison of Tumor volume between Vehicle and CX-4945 treated mice A673 cells **(right panel)** and PDX 1460 cells **(left panel); (C)** Comparison of survival between vehicle and CX-4945 treated mice A673 cells **(right panel)** and PDX 1460 cells **(left panel); (D-E)** Tumor pictures **(D)** and Tumor volume **(E),** were recorded after collecting the tumor from the mice A673 cells **(right panel)** and PDX 1460 cells **(left panel); (F)** H&E and IHC staining showing the difference between vehicle and CX-4945 treated mice, tumor tissues **(left panel)** and lungs tissues **(right panel)** stained with CD99 and Ki67, A673 cells**.**

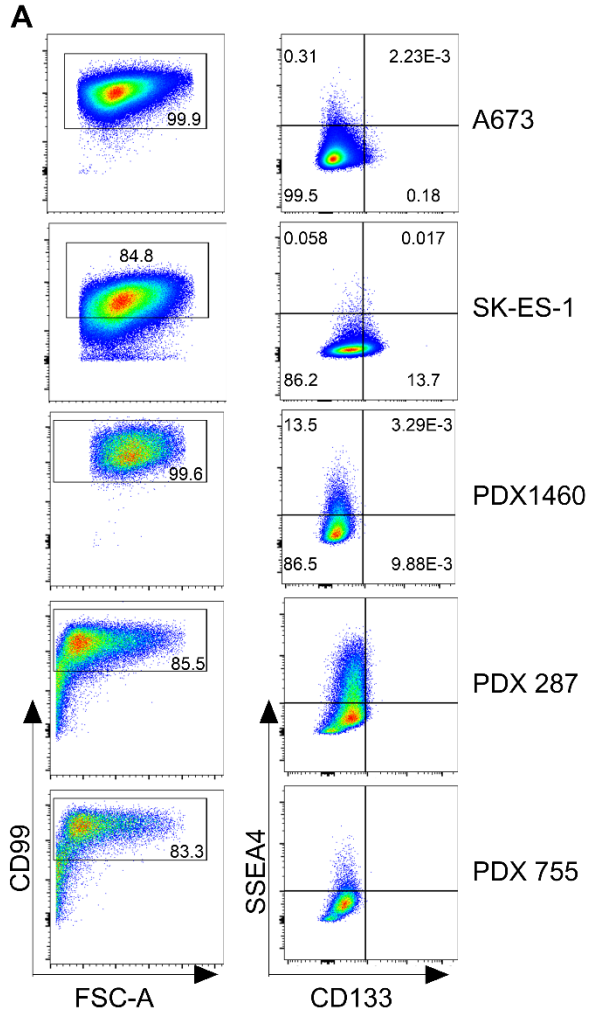
A
99.9
0.31
2.23E-3
99.5
0.18
A673
84.8
0.058
0.017
86.2
13.7
SK-ES-1
99.6
13.5
3.29E-3
86.5
9.88E-3
PDX1460
85.5
PDX 287
83.3
PDX 755
CD99
SSEA4
FSC-A
CD133

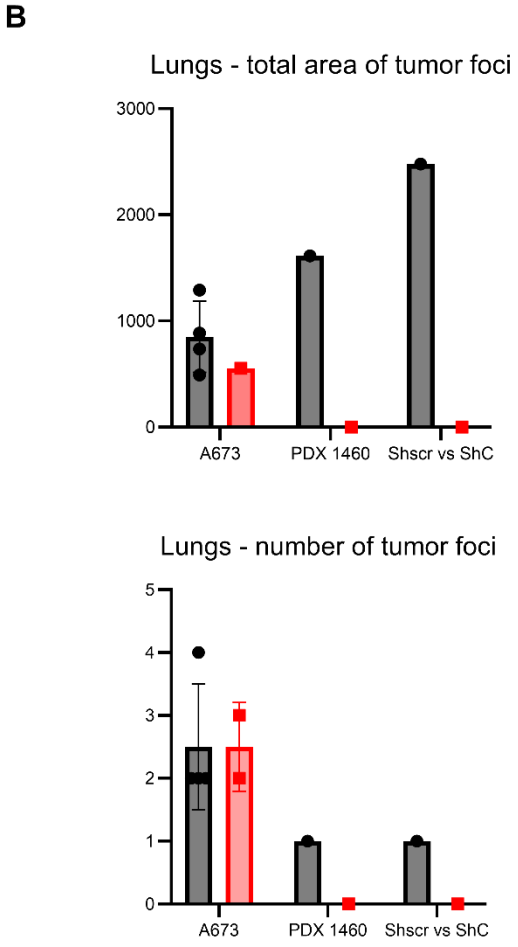
B
Lungs - total area of tumor foci
3000
2000
1000
0
A673
PDX 1460
Shscr vs ShC
Lungs - number of tumor foci
5
4
3
2
1
0
A673
PDX 1460
Shscr vs ShC

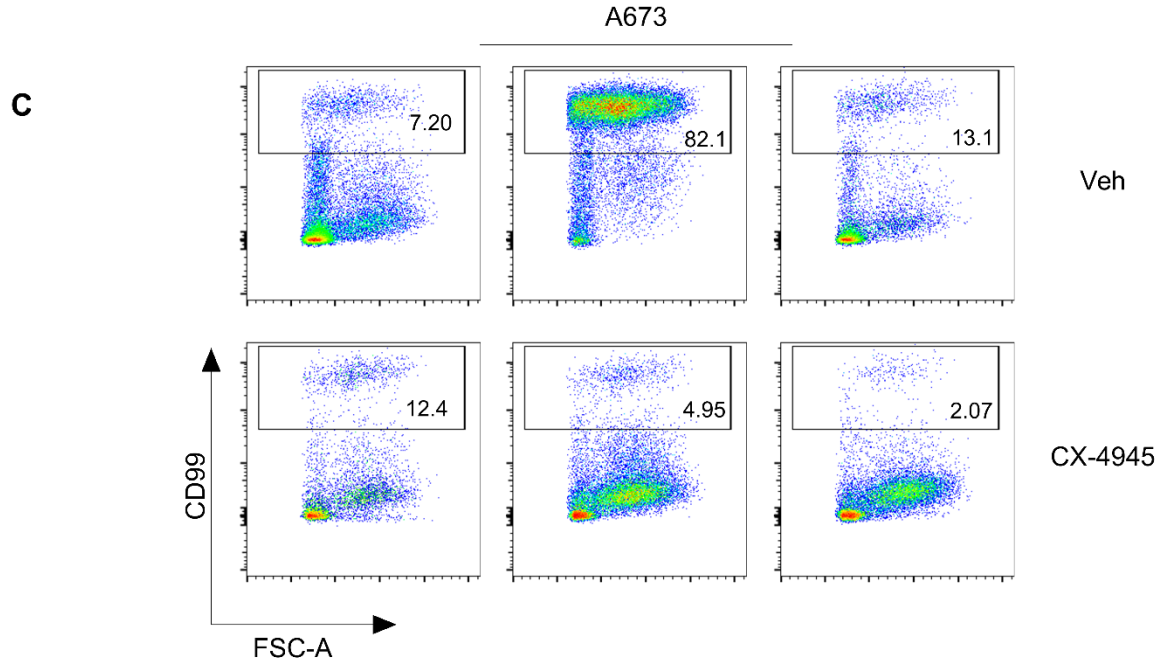
C
A673
7.20
82.1
13.1
Veh
12.4
4.95
2.07
CX-4945
CD99
FSC-A

Figure 7: Characterization and metastatic analysis of Ewing sarcoma PDX and cell line by flow cytometry: (A) Baseline characterization of 3 Ewing sarcoma PDX and 2 cell lines; all the cell lines and PDX stained with zombie aqua, CD99, CD133 and SSEA4 and analysis for the surface antigen through flow cytometry **(B)** Analysis of Ewing sarcoma, lung metastasis through H&E stained slides of A673, PDX1460 and Sh-Scr vs Sh-C. Lung tissue were collected at the end point and fixed and embedded in paraffin blocks, tissue section slides were prepared form paraffin blocks and stained for H&E staining and analysis by pathologist. **(C)** Flow analysis of hCD99 marker in single cells, collected from the mice lungs, at the end point from the Veh and CX-4945 treated groups.

Conclusion:

In summary, we have shown that, CK2 inhibition decreases EWS-FLI1 protein abundance, likely due to increased ubiquitination and proteasome-mediated degradation. Oral, single-agent CX-4945 treatment in EWS-FLI1 EWS xenografts decreased tumor growth and significantly improved survival. CX-4945 treated EWS tumors show decreased EWS-FLI1 protein and CK2 substrate phosphorylation. Completed and ongoing phase 1 clinical trials in adult and pediatric cancers provide safety, tolerability, and an adult-recommended Phase-2 dose.

The combination of CX-4945 with cytotoxic drugs in EWS targeting the EWS-FLI1 pathway has never been tested before. This novel combination therapy is being tested in an ongoing clinical trial. These results provide a mechanistic rationale for testing the CK2 inhibitor to target EWS-FLI1 in EWS.

References:

1. Siegel RL, Miller KD, Jemal A. Cancer statistics, 2020. CA Cancer J Clin. 2020 01;70(1):7-30. PubMed PMID: 31912902. Epub 2020/01/08. eng.

2. Grünewald TGP, Cidre-Aranaz F, Surdez D, Tomazou EM, de Álava E, Kovar H, et al. Ewing sarcoma. Nat Rev Dis Primers. 2018 Jul 5;4(1):5. PubMed PMID: 29977059. Epub 20180705. eng.

3. Delattre O, Zucman J, Plougastel B, Desmaze C, Melot T, Peter M, et al. Gene fusion with an ETS DNA-binding domain caused by chromosome translocation in human tumours. Nature. 1992 Sep 10;359(6391):162-5. PubMed PMID: 1522903. eng.

4. Van Mater D, Wagner L. Management of recurrent Ewing sarcoma: challenges and approaches. Onco Targets Ther. 2019;12:2279-88. PubMed PMID: 30988632. PMCID: PMC6441548. Epub 20190327. eng.

5. Leavey PJ, Mascarenhas L, Marina N, Chen Z, Krailo M, Miser J, et al. Prognostic factors for patients with Ewing sarcoma (EWS) at first recurrence following multi-modality therapy: A report from the Children's Oncology Group. Pediatr Blood Cancer. 2008 Sep;51(3):334-8. PubMed PMID: 18506764. PMCID: PMC2728357. eng.

6. Collier AB, 3rd, Krailo MD, Dang HM, DuBois SG, Hawkins DS, Bernstein ML, et al. Outcome of patients with relapsed or progressive Ewing sarcoma enrolled on cooperative group phase 2 clinical trials: A report from the Children's Oncology Group. Pediatr Blood Cancer. 2021 Dec;68(12):e29333. PubMed PMID: 34496122. PMCID: PMC8541905. Epub 20210908. eng.

7. Bailly RA, Bosselut R, Zucman J, Cormier F, Delattre O, Roussel M, et al. DNA-binding and transcriptional activation properties of the EWS-FLI-1 fusion protein resulting from the t(11;22) translocation in Ewing sarcoma. Mol Cell Biol. 1994 May;14(5):3230-41. PubMed PMID: 8164678. PMCID: PMC358690. eng.

8. Showpnil IA, Selich-Anderson J, Taslim C, Boone MA, Crow JC, Theisen ER, et al. EWS/FLI mediated reprogramming of 3D chromatin promotes an altered transcriptional state in Ewing sarcoma. Nucleic Acids Res. 2022 Sep 23;50(17):9814-37. PubMed PMID: 36124657. PMCID: PMC9508825. eng.

9. Riggi N, Knoechel B, Gillespie SM, Rheinbay E, Boulay G, Suvà ML, et al. EWS-FLI1 utilizes divergent chromatin remodeling mechanisms to directly activate or repress enhancer elements in Ewing sarcoma. Cancer Cell. 2014 Nov 10;26(5):668-81. PubMed PMID: 25453903. PMCID: PMC4492343. Epub 20141030. eng.

10. Su S, Chen J, Jiang Y, Wang Y, Vital T, Zhang J, et al. SPOP and OTUD7A Control EWS-FLI1 Protein Stability to Govern Ewing Sarcoma Growth. Adv Sci (Weinh). 2021 Jul;8(14):e2004846. PubMed PMID: 34060252. PMCID: PMC8292909. Epub 20210601. eng.

11. St-Denis NA, Litchfield DW. Protein kinase CK2 in health and disease: From birth to death: the role of protein kinase CK2 in the regulation of cell proliferation and survival. Cell Mol Life Sci. 2009 Jun;66(11-12):1817-29. PubMed PMID: 19387552. eng.

12. Turowec JP, Duncan JS, French AC, Gyenis L, St Denis NA, Vilk G, et al. Protein kinase CK2 is a constitutively active enzyme that promotes cell survival: strategies to identify CK2 substrates and manipulate its activity in mammalian cells. Methods Enzymol. 2010;484:471-93. PubMed PMID: 21036246. eng.

13. Strum SW, Gyenis L, Litchfield DW. CSNK2 in cancer: pathophysiology and translational applications. British Journal of Cancer. 2022 2022/04/01;126(7):994-1003.

14. Chandrika G, Mansi S, Sunil M, Malika K, Lidija P-D, Melanie H, et al. Casein kinase II (CK2) as a therapeutic target for hematological malignancies. Current Pharmaceutical Design. 2016;22:1-13.

15. Ahmad KA, Wang G, Slaton J, Unger G, Ahmed K. Targeting CK2 for cancer therapy. Anticancer Drugs. 2005 Nov;16(10):1037-43. PubMed PMID: 16222144. eng.

16. Borgo C, Ruzzene M. Role of protein kinase CK2 in antitumor drug resistance. J Exp Clin Cancer Res. 2019 Jul;38(1):287. PubMed PMID: 31277672. PMCID: PMC6612148. Epub 2019/07/05. eng.

17. Borgo C, D'Amore C, Sarno S, Salvi M, Ruzzene M. Protein kinase CK2: a potential therapeutic target for diverse human diseases. Signal Transduction and Targeted Therapy. 2021 2021/05/17;6(1):183.

18. Buontempo F, McCubrey JA, Orsini E, Ruzzene M, Cappellini A, Lonetti A, et al. Therapeutic targeting of CK2 in acute and chronic leukemias. Leukemia. 2018 01;32(1):1-10. PubMed PMID: 28951560. PMCID: PMC5770594. Epub 2017/09/27. eng.

19. Bortolato A, Cozza G, Moro S. Protein kinase CK2 inhibitors: emerging anticancer therapeutic agents? Anticancer Agents Med Chem. 2008 Oct;8(7):798-806. PubMed PMID: 18855581. eng.

20. Cozza G, Bortolato A, Moro S. How druggable is protein kinase CK2? Med Res Rev. 2010 May;30(3):419-62. PubMed PMID: 19526464. eng.

21. D'Amore C, Borgo C, Sarno S, Salvi M. Role of CK2 inhibitor CX-4945 in anti-cancer combination therapy – potential clinical relevance. Cellular Oncology. 2020 2020/12/01;43(6):1003-16.

22. Chon HJ, Bae KJ, Lee Y, Kim J. The casein kinase 2 inhibitor, CX-4945, as an anti-cancer drug in treatment of human hematological malignancies. Front Pharmacol. 2015;6:70. PubMed PMID: 25873900. PMCID: PMC4379896. eng.

23. Pierre F, Chua PC, O'Brien SE, Siddiqui-Jain A, Bourbon P, Haddach M, et al. Pre-clinical characterization of CX-4945, a potent and selective small molecule inhibitor of CK2 for the treatment of cancer. Mol Cell Biochem. 2011 Oct;356(1-2):37-43. PubMed PMID: 21755459. eng.

24. Beauchamp E, Bulut G, Abaan O, Chen K, Merchant A, Matsui W, et al. GLI1 is a direct transcriptional target of EWS-FLI1 oncoprotein. J Biol Chem. 2009 Apr 3;284(14):9074-82. PubMed PMID: 19189974. PMCID: PMC2666556. Epub 20090203. eng.

25. Litchfield DW. Protein kinase CK2: structure, regulation and role in cellular decisions of life and death. Biochem J. 2003 Jan;369(Pt 1):1-15. PubMed PMID: 12396231. PMCID: PMC1223072. eng.

26. Chua MM, Ortega CE, Sheikh A, Lee M, Abdul-Rassoul H, Hartshorn KL, et al. CK2 in Cancer: Cellular and Biochemical Mechanisms and Potential Therapeutic Target. Pharmaceuticals

(Basel). 2017 Jan;10(1). PubMed PMID: 28134850. PMCID: PMC5374422. Epub 2017/01/28. eng.

27. Lou DY, Dominguez I, Toselli P, Landesman-Bollag E, O'Brien C, Seldin DC. The alpha catalytic subunit of protein kinase CK2 is required for mouse embryonic development. Mol Cell Biol. 2008 Jan;28(1):131-9. PubMed PMID: 17954558. PMCID: PMC2223292. Epub 2007/10/22. eng.

28. Kramerov AA, Ljubimov AV. Focus on molecules: protein kinase CK2. Exp Eye Res. 2012 Aug;101:111-2. PubMed PMID: 21194531. PMCID: PMC3437250. Epub 20101229. eng.

29. Litchfield DW, Bosc DG, Canton DA, Saulnier RB, Vilk G, Zhang C. Functional specialization of CK2 isoforms and characterization of isoform-specific binding partners. Mol Cell Biochem. 2001 Nov;227(1-2):21-9. PubMed PMID: 11827170. eng.

30. Meggio F, Pinna LA. One-thousand-and-one substrates of protein kinase CK2? FASEB J. 2003 Mar;17(3):349-68. PubMed PMID: 12631575. eng.

31. Roffey SE, Litchfield DW. CK2 Regulation: Perspectives in 2021. Biomedicines. 2021 Sep 30;9(10). PubMed PMID: 34680478. PMCID: PMC8533506. Epub 20210930. eng.

32. Trembley JH, Chen Z, Unger G, Slaton J, Kren BT, Van Waes C, et al. Emergence of protein kinase CK2 as a key target in cancer therapy. Biofactors. 2010 2010 May-Jun;36(3):187-95. PubMed PMID: 20533398. PMCID: PMC2916697. eng.

33. Trembley JH, Kren BT, Afzal M, Scaria GA, Klein MA, Ahmed K. Protein kinase CK2 - diverse roles in cancer cell biology and therapeutic promise. Mol Cell Biochem. 2022 Sep 17:1-28. PubMed PMID: 36114992. PMCID: PMC9483426. Epub 20220917. eng.

34. Ortega CE, Seidner Y, Dominguez I. Mining CK2 in cancer. PLoS One. 2014;9(12):e115609. PubMed PMID: 25541719. PMCID: PMC4277308. Epub 2014/12/26. eng.

35. Chen H, Liu H, Qing G. Targeting oncogenic Myc as a strategy for cancer treatment. Signal Transduction and Targeted Therapy. 2018 2018/02/23;3(1):5.

36. Pierre F, Chua PC, O'Brien SE, Siddiqui-Jain A, Bourbon P, Haddach M, et al. Discovery and SAR of 5-(3-chlorophenylamino)benzo[c][2,6]naphthyridine-8-carboxylic acid (CX-4945), the first clinical stage inhibitor of protein kinase CK2 for the treatment of cancer. J Med Chem. 2011 Jan 27;54(2):635-54. PubMed PMID: 21174434. Epub 20101221. eng.

37. Battistutta R, Cozza G, Pierre F, Papinutto E, Lolli G, Sarno S, et al. Unprecedented selectivity and structural determinants of a new class of protein kinase CK2 inhibitors in clinical trials for the treatment of cancer. Biochemistry. 2011 Oct;50(39):8478-88. PubMed PMID: 21870818. eng.